10.1109/ULTSYM.2013.0349

Full-wave Nonlinear Ultrasound Simulation in an Axisymmetric Coordinate System Using the Discrete Sine and Cosine Transforms

Elliott S. Wise*†, Bradley E. Treeby*‡
†Computational Informatics, Commonwealth Scientific and Industrial Research Organisation, Melbourne, Australia
‡Department of Medical Physics and Bioengineering, University College London, London, United Kingdom
†Email: elliott.wise@csiro.au ‡Email: b.treeby@ucl.ac.uk

***Abstract*—The simulation of ultrasound propagation through biological tissue has a wide range of applications in medicine. However, ultrasound simulation presents a computationally difficult problem, as simulation domains are very large compared with the acoustic wavelengths of interest. This becomes a greater problem when simulating high intensity focussed ultrasound since nonlinear effects increase the required resolution of computational grids. Two common methods for dealing with this difficulty include using spectral methods for solving the acoustic model equations and using an axisymmetric assumption for the system. In this paper, a full-wave nonlinear model similar to the Westervelt equation is solved using pseudospectral methods based on the discrete sine and cosine transforms. These methods can be used to apply homogeneous Neumann and Dirichlet boundary conditions (both of which are present in axisymmetric systems) while retaining the many established benefits of the Fourier spectral method. The accuracy of the model is established through comparison with analytical solutions to several nonlinear wave equations.**

I. Introduction

The simulation of ultrasound propagation plays an important role in the development of technologies such as photoacoustic tomography and high intensity focussed ultrasound (HIFU). These simulations need to account for a range of effects seen in biological tissue such as acoustic absorption and nonlinear propagation. These effects are particularly important in HIFU since nonlinear propagation results from high acoustic pressures and acoustic absorption causes significant heating in tissue. High pressures additionally create steep wavefronts and short acoustic wavelengths, which require dense computational grids and correspondingly high levels of computational resources.

One simplification that is commonly made in ultrasound simulations is to assume axisymmetry in the system. A prominent nonlinear axisymmetric method was developed by Lee and is found in the KZKTexas code [1]. This method solves the KZK equation and models the propagation of pulsed sound beams in homogeneous, thermoviscous fluids. The KZK equation only permits one-way propagation of waves however, and so cannot be extended to include tissue heterogeneities since these produce reflections. Sparrow & Raspet [2] and Hallaj & Cleveland [3] both solve full-wave axisymmetric models that do not have these limitations. Their models are solved using finite-difference methods however, which require many computational grid points per acoustic wavelength. In comparison, spectral methods converge exponentially and only require close to the Nyquist limit of two points per wavelength. An example of a full-wave nonlinear spectral method is provided by Albin et al. in which the Fourier Continuation method is applied to ultrasound simulation [4]. The Fourier Continuation method deals with the symmetric extension through the system's axis by mirroring a strip of points beyond the simulation domain, rather than through the direct application of an appropriate boundary condition.

The present paper solves a full-wave acoustic model using a spectral method based on the discrete sine and cosine transforms which is capable of dealing with symmetrically and antisymmetrically extended computational domains. The acoustic model has been developed by Treeby et al. for Cartesian systems and is composed of three coupled first-order partial differential equations, together equivalent to a generalised Westervelt equation [5], [6]. This model includes the effects of tissue heterogeneities (sound speed, density, and nonlinearity) and thermoviscous absorption. Some of the spectral methods provided here have seen some use in the past by Kosloff & Kosloff in solving the wave equation with reflective boundaries, and by Long & Rheinhard in solving the Navier-Stokes equation to constrain fluid flow within a tank [7], [8]. Their use there reflected their ability to apply homogeneous Neumann and Dirichlet boundary conditions to the solution of partial differential equations.

II. The Westervelt Equation in an Axisymmetric System

The model used in this paper consists of a system of three first-order partial differential equations in three acoustic variables, which together combine to give the Westervelt equation. Using a system of equations for each variable gives a number of benefits, including allowing quantities such as the acoustic intensity and the heating of tissue to be calculated from the acoustic field variables, permitting staggered time and spatial grids to be used to improve the accuracy of numerical methods, and simplifying the addition of force and mass sources. Following Treeby et al. [6] the system of equations is

$$\frac{\partial \mathbf{u}}{\partial t} = -\frac{1}{\rho_0}\nabla p + \mathbf{S}_{\mathrm{F}} \ , \qquad \text{(cons. momentum)} \quad (1)$$

$$\frac{\partial \rho}{\partial t} = -(2\rho + \rho_0)\nabla \cdot \mathbf{u} + \mathrm{S}_{\mathrm{M}} \ , \qquad \text{(cons. mass)} \quad (2)$$

$$p = c_0^2 \left(\rho + \frac{B}{2A}\frac{\rho^2}{\rho_0} - \mathrm{L}\rho \right) \ . \qquad \text{(eq. of state)} \quad (3)$$

*E. Wise and B. Treeby were previously with the Research School of Engineering, Australian National University, Canberra, Australia.

Here ρ_0 and c_0 are the ambient density and sound speed, and $\mathbf{S}_\mathrm{F}$ and S_M are force and mass sources. The ratio B/A characterises the relative contribution of finite-amplitude effects to the sound speed, and the term $-2\rho\nabla\cdot\mathbf{u}$ in Eq. (2) describes the contribution of the particle velocity to the wave velocity. The loss operator L is defined as

$$\mathrm{L} = -2\alpha_0 c_0 \frac{\partial}{\partial t} \ , \tag{4}$$

where α_0 is the power law prefactor and absorption follows a frequency squared power law.

Solving these equations in an axisymmetric system requires the axisymmetric forms of the gradient and divergence operators. In the context of Eqs. (1) and (2) these are

$$\nabla p = \frac{\partial}{\partial r}\hat{r} + \frac{\partial}{\partial z}\hat{z} \ , \tag{5}$$

$$\nabla\cdot\mathbf{u} = \frac{u_r}{r} + \frac{\partial u_r}{\partial r} + \frac{\partial u_z}{\partial z} \ . \tag{6}$$

The $1/r$ term that occurs in the divergence equation is important since this restricts us to calculating Eq. (6) at points that aren't on the system's axis. To do this, a staggered grid scheme is used where p and ρ are defined on a grid that includes the axis while $\mathbf{u}$ is defined on a grid shifted by half the grid point spacing. This is indeed one motivation for using a split form of the wave equation as the Laplacian operator that occurs in the general second-order wave equation includes a $1/r$ term preventing the pressure field from being calculated on the axis. Defining p along the axis is important for modelling the response of transducers since the maximal pressure occurs on (or at least near) the axis and is needed for calculating the heat delivered to tissue at the transducer's focal point.

III. Axisymmetric Boundary Conditions

To simulate free-field conditions a perfectly matched layer (PML) is used to absorb the waves at the simulation boundaries [9]. In a Cartesian system a PML would be placed on all boundaries to prevent reflections, however in the axisymmetric case symmetry allows our simulation to have one boundary placed on the system's axis with the wave field mirrored beyond it, and so only three PMLs are used. This mirroring is equivalent to applying a symmetric extension in the radial direction to p, u_z and ρ, and to applying an antisymmetric extension to u_r. To illustrate this, the acoustic pressure field for the simulation in Sec. VI-B is shown in Fig. 1.

These antisymmetric and symmetric extensions can be implemented by applying homogeneous Neumann and Dirichlet boundary conditions on the axis. The implementation of these conditions in a spectral method is often done using a polynomial basis defined on a Chebychev grid. The Chebychev grid has the disadvantage however of needing a higher density of points near the simulation boundaries and having a much stricter stability requirement. For a given maximum grid spacing a Chebychev grid requires $(\pi/2)^D$ more grid points where D is the dimension of the simulation. It would be preferable instead to be able to use an equispaced grid, like that available through Fourier spectral methods. However to do so requires the inherent periodicity of Fourier spectral methods to be dealt with.

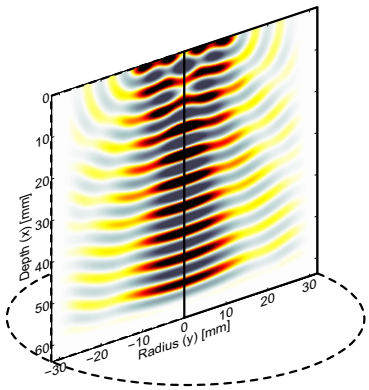

Fig. 1. Simulated acoustic pressure field for an unfocussed cylindrical transducer. The field is calculated for positive radial coordinates and a symmetric boundary condition is used to imply the mirroring beyond the axis.

IV. Symmetric and Antisymmetric Fourier Spectral Methods

A general approach to implementing Neumann and Dirichlet boundary conditions in a spectral method is to choose basis functions that implicitly meet those conditions [10, p.135]. One appropriate choice of basis functions are sines and cosines respectively – noting unlike a Fourier representation that the choice needs to be mutually exclusive (i.e *only* sines or *only* cosines). Much like a Fourier spectral method we can represent a sampled function u of length N by a weighted sum of sinusoids defined for a set of equally spaced wavenumbers k_n. That is either

$$u_j = \sum_n A_n \sin\left(k_n x_j\right) \ , \text{ or} \tag{7}$$

$$u_j = \sum_n B_n \cos\left(k_n x_j\right) \ , \tag{8}$$

where A_n and B_n are the weights associated with each basis function and $j, n = 1, 2, \ldots, N$.

To determine these weights and wavenumbers we use the discrete sine and cosine transforms, collectively referred to as the discrete trigonometric transforms (DTTs). There are sixteen DTTs, each corresponding to a specific type of discrete symmetry on the left and right boundaries. Symmetry may be either symmetric (S) or antisymmetric (A) and the point of symmetry may lie on a data point (W) or halfway between data points (H). The DTTs can be labelled by the symmetry on each boundary, for instance a Dirichlet condition applied at a data point on the left boundary and a Neumann condition applied halfway between data points on the right boundary would be labelled as WSHA. Table I provides these boundary symmetries along with their corresponding DTTs and wavenumber sets[1]. In it, N is the length of the representative sample of the sequence the DTT is applied to and M is the implied periodic length of the sequence. The DTTs can be divided into four classes based on whether their implied periodic length M is an even or odd number (even and odd classes), and whether

[1]See Martucci for an explanation of the DTTs and their relationships to one-another and to the generalised Fourier transform [11]. As in this paper, Martucci notes the existence of four DTT classes based on wavenumbers, though in the context of convolution rather than differentiation.

TABLE I. THE DISCRETE TRIGONOMETRIC TRANSFORM CLASSES

Wavenumbers	Symmetry	DTT	$n = \ldots$	$M = \ldots$
$k_n = \frac{2\pi}{M\Delta x} n$	WSWS	$\mathbb{C}_1$	$0, 1, \ldots, \frac{M}{2}$	$2(N-1)$
	HSHS	$\mathbb{C}_2$	$0, 1, \ldots, \frac{M}{2} - 1$	$2N$
	WAWA	$\mathbb{S}_1$	$1, 2, \ldots, \frac{M}{2} - 1$	$2(N+1)$
	HAHA	$\mathbb{S}_2$	$1, 2, \ldots, \frac{M}{2}$	$2N$
	WSHS	$\mathbb{C}_5$	$0, 1, \ldots, \frac{M-1}{2}$	$2N-1$
	HSWS	$\mathbb{C}_6$	$0, 1, \ldots, \frac{M-1}{2}$	$2N-1$
	WAHA	$\mathbb{S}_5$	$1, 2, \ldots, \frac{M+1}{2}$	$2N+1$
	HAWA	$\mathbb{S}_6$	$1, 2, \ldots, \frac{M+1}{2}$	$2N+1$
$k_n = \frac{2\pi}{M\Delta x} (n + \frac{1}{2})$	WSWA	$\mathbb{C}_3$	$0, 1, \ldots, \frac{M}{2} - 1$	$2N$
	HSHA	$\mathbb{C}_4$	$0, 1, \ldots, \frac{M}{2} - 1$	$2N$
	WAWS	$\mathbb{S}_3$	$0, 1, \ldots, \frac{M}{2} - 1$	$2N$
	HAHS	$\mathbb{S}_4$	$0, 1, \ldots, \frac{M}{2} - 1$	$2N$
	WSHA	$\mathbb{C}_7$	$0, 1, \ldots, \frac{M-1}{2}$	$2N-1$
	HSWA	$\mathbb{C}_8$	$0, 1, \ldots, \frac{M-1}{2}$	$2N+1$
	WAHS	$\mathbb{S}_7$	$0, 1, \ldots, \frac{M-1}{2}$	$2N+1$
	HAWS	$\mathbb{S}_8$	$0, 1, \ldots, \frac{M-1}{2}$	$2N-1$

their wavenumbers are shifted by $\pi/M\Delta x$ (whole- and half-wavenumber classes).

To form a pseudospectral method we make use of the same frequency-space differentiation properties that make the Fourier spectral method possible, namely

$$\frac{\partial}{\partial x} A_n \sin(k_n x) = k_n A_n \cos(k_n x) \ , \text{ and} \tag{9}$$

$$\frac{\partial}{\partial x} B_n \cos(k_n x) = -k_n B_n \sin(k_n x) \ . \tag{10}$$

Thus, a DTT spectral method involves transforming a discretely sampled function u into frequency space using a DTT appropriate to the sequence's boundary conditions, scaling the basis function weights (A_n or B_n) by their wavenumbers (k_n or $-k_n$), and inverting the derivative back using an inverse DTT corresponding to the boundary conditions of the differentiated function u'. That is, either

$$u' \approx \mathbb{S}^{-1}\{k\mathbb{C}\{u\}\} \ , \text{ or} \tag{11}$$

$$u' \approx \mathbb{C}^{-1}\{-k\mathbb{S}\{u\}\} \ . \tag{12}$$

where $\mathbb{S}$ and $\mathbb{C}$ are the discrete sine and cosine transforms. Note that under differentiation symmetry about a boundary will change from symmetric to antisymmetric and vice-versa. There are two options available when choosing the inverse DTT – the differentiated sequence can be reconstructed on the original sampling grid or on a staggered grid. This is possible because each DTT class includes transforms defined for subsets of the same set of basis wavenumbers, but for differing symmetry types and spatial grids. When forming DTT pseudospectral methods, a key consideration that arises is that the forward and inverse subsets of wavenumbers may differ. This is dealt with by trimming any extra basis function weights and setting any missing ones to zero before inversion.

V. DISCRETE MODEL EQUATIONS

The ultrasound model given in Eqs. (1)–(3) is solved using DTT pseudospectral methods from the even half-wavenumber class along with a centred leapfrog time scheme. On the non-axis boundaries any symmetry applied will be negated by a PML, and so can be chosen arbitrarily. Thus, p and ρ are given WSWA boundaries in both the radial and depth dimensions (the axis is on the left radial boundary) and u_r and u_z have HAHS boundaries. This is shown in Fig. 2. By choosing a half-wavenumber DTT class we have avoided trimming or zero-padding sequences in frequency space since all DTTs in each half-wavenumber class are defined for the same subset of wavenumbers. Choosing an even class gives access to the fast algorithms available through the FFTW library [12]. The model was implemented in MATLAB using a mex interface to FFTW as an extension to the MATLAB *k*-Wave toolbox [5]. The PML is not included in the equations below for simplicity, however it is applied by simply scaling $\mathbf{u}$ and ρ at each time step.

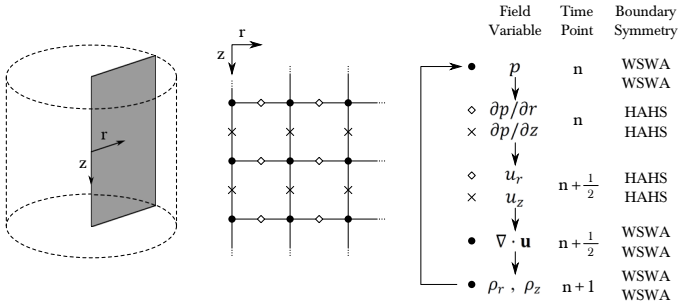

Fig. 2. The axisymmetric coordinate system used showing the grids on which field variables are calculated and the time steps at which they are defined.

To begin, Eq. (1) is calculated in two parts as

$$\frac{\partial}{\partial \xi} p^n = \mathbb{S}_4^{-1}\{-k_\xi \mathbb{C}_3\{p^n\}\} \ , \tag{13}$$

$$u_\xi^{n+\frac{1}{2}} = u_\xi^{n-\frac{1}{2}} - \frac{\Delta t}{\rho_0} \frac{\partial}{\partial \xi} p^n + \Delta t \mathrm{S}_{\mathrm{F}_\xi}^n \ , \tag{14}$$

where $\xi = r, z$ and n is the current timestep. The acoustic density is split into two components so that the PML can be applied and as a result the radial terms in the divergence operator from Eq. (6) are calculated separately from the depth term. Noting that u_r/r has HSHA-type boundaries, we calculate the radial and depth components of the divergence term as

$$\left(\nabla \cdot \mathbf{u}^{n+\frac{1}{2}}\right)_r = \mathbb{C}_3^{-1}\left\{\mathbb{C}_4\left\{\frac{u_r^{n+\frac{1}{2}}}{r}\right\} + k_r \mathbb{S}_4\left\{u_r^{n+\frac{1}{2}}\right\}\right\} \ , \tag{15}$$

$$\left(\nabla \cdot \mathbf{u}^{n+\frac{1}{2}}\right)_z = \mathbb{C}_3^{-1}\left\{k_z \mathbb{S}_4\left\{u_z^{n+\frac{1}{2}}\right\}\right\} \ . \tag{16}$$

Here u_r/r has been transformed into frequency space so that it can be shifted onto a whole-sample grid after being added to $\partial u_r/\partial r$. These can be added to the radial and depth components of the acoustic density, solving Eq. (2) as

$$\rho_\xi^{n+1} = \frac{\rho_\xi^n - \Delta t \rho_0 \left(\nabla \cdot \mathbf{u}^{n+\frac{1}{2}}\right)_\xi + \Delta t \mathrm{S}_{\mathrm{M}_\xi}^{n+\frac{1}{2}}}{1 + 2\Delta t \left(\nabla \cdot \mathbf{u}^{n+\frac{1}{2}}\right)_\xi} \ , \tag{17}$$

where $\xi = r, z$. The two density components are then recombined to give the total acoustic density

$$\rho^{n+1} = \rho_r^{n+1} + \rho_z^{n+1} \ . \tag{18}$$

Finally, the pressure–density relation from Eq. (3) is discretised as

$$p^{n+1} = c_0^2 \left(\rho^{n+1} + \frac{B}{2A} \frac{1}{\rho_0} \left(\rho^{n+1} \right)^2 - \mathrm{L_d} \right) \quad , \tag{19}$$

with the loss operator given by

$$\begin{aligned} \mathrm{L_d} &= -2\alpha_0 c_0 \frac{\partial}{\partial t} \rho^{n+1} \\ &= -2\alpha_0 c_0 \rho_0 \left(\left(\frac{1}{r} + \frac{\partial}{\partial r} \right) u_r^{n+\frac{1}{2}} + \frac{\partial}{\partial z} u_z^{n+\frac{1}{2}} \right) \quad , \end{aligned} \tag{20}$$

Here, the term $\frac{\partial}{\partial t}\rho^{n+1}$ has been expanded using Eq. (2) prior to the leapfrog time scheme being applied to integrate it.

VI. Numerical Validation

A. Nonlinear Propagation and Thermoviscous Absorption

When acoustic waves possess a high amplitude to wavelength ratio nonlinear propagation effects are seen, producing steep wavefronts. To see the accuracy of the axisymmetric model and pseudospectral method given in this paper, a comparison is drawn with an analytical solution to the Burgers equation [13]. This solution is for a monochromatic plane wave which is simulated propagating 15 wavelengths along the system's axis. The results are given in Fig. 3 where a good agreement is evident between the simulated and analytical solutions.

B. Comparison with the Rayleigh Integral and KZK Equation

The KZK equation is often used to model nonlinear acoustics with thermoviscous absorption, notably in the KZKTexas code [1]. Lee has analytically solved a linearised form of the KZK equation for the maximal acoustic pressure along the axis for an unfocussed monochromatic cylindrical transducer, however this solution includes a singularity at the transducer [1]. Pierce has derived an analytical solution to the Rayleigh integral for the same system, but without the erroneous behaviour at the transducer [14]. Fig. 3 shows a comparison between the simulated system and these solutions. The simulation agrees closely with the Rayleigh integral, while the singularity in the KZK equation solution manifests as a high frequency oscillation near the transducer, and accuracy is only achieved at points in the far-field, beyond the dotted vertical line.

VII. Conclusion

An axisymmetric ultrasound model has been presented that efficiently and accurately accounts for nonlinear propagation effects and thermoviscous absorption. The discrete sine and cosine transforms are used to solve this model since they provide fast pseudospectral methods capable of applying homogeneous Dirichlet and Neumann boundary conditions. Nonlinear propagation and absorption effects are validated using an analytical solution to the Burgers equation and a favourable comparison is made with the one-way KZK equation. The model presented has applications in high intensity focussed ultrasound where it can simulate reflections and scattering in heterogeneous tissue.

Acknowledgment

This work was supported in part by the Australian Research Council/Microsoft Linkage Project LP100100588.

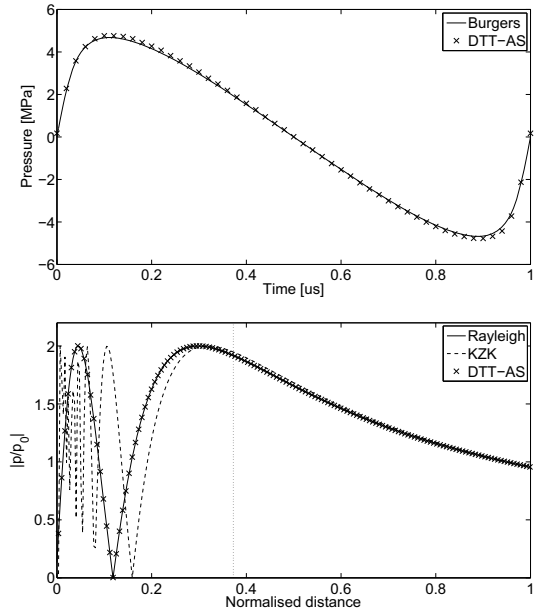

Fig. 3. Validation of the axisymmetric DTT model. (Top) Nonlinear effects are compared with the Burgers equation. (Bottom) The axial pressure from a transducer is compared with the Rayleigh integral and KZK equation.

References

[1] Y.-S. Lee, "Numerical solution of the KZK equation for pulsed finite amplitude sound beams in thermoviscous fluids," Ph.D. dissertation, The University of Texas at Austin, 1993.

[2] V. Sparrow and R. Raspet, "A numerical method for general finite amplitude wave propagation in two dimensions and its application to spark pulses," *J. Acoust. Soc. Am.*, vol. 90, no. 5, pp. 2683–2691, 1991.

[3] I. Hallaj and R. Cleveland, "FDTD simulation of finite-amplitude pressure and temperature fields for biomedical ultrasound," *J. Acoust. Soc. Am.*, vol. 105, no. 5, 1999.

[4] N. Albin, et al. "Fourier continuation methods for high-fidelity simulation of nonlinear acoustic beams," *J. Acoust. Soc. Am.*, vol. 132, no. 4, pp. 2371–2387, 2012.

[5] B. E. Treeby and B. T. Cox, "k-Wave : MATLAB toolbox for the simulation and reconstruction of photoacoustic wave fields," *Journal of Biomedical Optics*, vol. 15, no. April, 2010.

[6] B. E. Treeby, J. Jaros, A. P. Rendell, and B. T. Cox, "Modeling nonlinear ultrasound propagation in heterogeneous media with power law absorption using a k-space pseudospectral method," *J. Acoust. Soc. Am.*, 2012.

[7] D. Kosloff and R. Kosloff, "A non-periodic Fourier method for solution of the classical wave equation," *Computer Physics Communications*, vol. 30, no. 3, pp. 333–336, Nov. 1983.

[8] B. Long and E. Reinhard, "Real-time fluid simulation using discrete sine/cosine transforms," *Proceedings of the 2009 symposium on Interactive 3D graphics and games*, no. 3, p. 99, 2009.

[9] J. Berenger, "A perfectly matched layer for the absorption of electromagnetic waves," *J. Comput. Phys.*, vol. 114, no. 2, pp. 185–200, 1994.

[10] L. N. Trefethen, *Spectral Methods in MATLAB*. SIAM, Philadelphia, 2000.

[11] S. Martucci, "Symmetric convolution and the discrete sine and cosine transforms," *IEEE Transactions on Signal Processing*, vol. 42, no. 5, pp. 1038–1051, 1994.

[12] M. Frigo and S. G. Johnson, "The Design and Implementation of FFTW3," *Proceedings of the IEEE*, vol. 93, pp. 216–231, 2005.

[13] J. S. Mendousse, "Nonlinear dissipative distortion of progressive sound waves at moderate amplitudes," *J. Acoust. Soc. Am.*, vol. 25, pp. 51–54, 1953.

[14] A. D. Pierce, *Acoustics: An Introduction to Its Physical Principles and Applications*. The Acoustical Society of America, 1991.